Lab on a Chip

TUTORIAL REVIEW

View Article Online
View Journal | View Issue

Cite this: *Lab Chip*, 2014, **14**, 4139

Deterministic lateral displacement for particle separation: a review

J. McGrath, M. Jimenez and H. Bridle*

Received 12th August 2014,
Accepted 4th September 2014

DOI: 10.1039/c4lc00939h

www.rsc.org/loc

Deterministic lateral displacement (DLD), a hydrodynamic, microfluidic technology, was first reported by Huang *et al.* in 2004 to separate particles on the basis of size in continuous flow with a resolution of down to 10 nm. For 10 years, DLD has been extensively studied, employed and modified by researchers in terms of theory, design, microfabrication and application to develop newer, faster and more efficient tools for separation of millimetre, micrometre and even sub-micrometre sized particles. To extend the range of potential applications, the specific arrangement of geometric features in DLD has also been adapted and/or coupled with external forces (*e.g.* acoustic, electric, gravitational) to separate particles on the basis of other properties than size such as the shape, deformability and dielectric properties of particles. Furthermore, investigations into DLD performance where inertial and non-Newtonian effects are present have been conducted. However, the evolvement and application of DLD has not yet been reviewed. In this paper, we collate many interesting publications to provide a comprehensive review of the development and diversity of this technology but also provide scope for future direction and detail the fundamentals for those wishing to design such devices for the first time.

Introduction

The emergence of the field of microfluidics was initially driven by the requirement for biomolecular analysis, however in more recent years microfluidic devices have extended their application to cell separation studies. Cell separation and manipulation is an essential sample processing step in many biological and medical assays[13] and the low Reynolds numbers, predictable flows, small dimensions, small fluid volumes plus the established microfabrication techniques and materials that are typical of microfluidic devices, allow the user to work at the scale of the cells.[14] Existing microfluidic, separation methods can be categorised as either active or passive,[13,15] where active methods incorporate an external force and passive methods rely on carefully designed channel geometries and internal forces to sort differing particles. Some common, active, separation methods include dielectrophoresis, electrophoresis, acoustophoresis, immunomagnetic separation (IMS), flow cytometry or FACS and optical force.[13,14,16] Alternatively, some passive methods adopted to differentiate between particles are the use of pillars, weirs and objects within microchannels, adhesion-based methods, pinched-flow fractionation (PFF), hydrodynamic filtration (HDF), hydrophoretic filtration, inertial forces and biomimetic separation.[13,15] Parameters such as size, shape, deformability, compressibility and density plus the dielectric, magnetic and adhesive properties of particles have been utilised in order to facilitate separation.[13] The reader could refer to the referenced articles,[13,15,16] where active and passive separation methods and respective particle properties utilised are described in depth.

The purpose of this review is to focus on one of these passive techniques, the Deterministic Lateral Displacement (DLD). Deterministic lateral displacement was first reported by Huang *et al.* in 2004 to separate particles on the basis of size in continuous flow with a resolution of down to 10 nm.[1] Since invention, this technique has been used to separate millimetre,[2] micrometre[3–7] and even sub-micrometre[1] sized particles and has been applied to diverse purposes, although mostly medical related (separation of trypanosomes,[17] white blood cells (WBCs),[6] red blood cells (RBCs),[9] circulating tumour cells[18] (CTCs) or platelets[19] from blood for instance). To extend the range of potential applications, the specific arrangement of geometric features in DLD has also been adapted and/or coupled with external forces (*e.g.* acoustic,[8] electric,[4,9] gravitational[10]) to separate particles on the basis of other properties than size such as the shape, deformability and dielectric properties of particles.

Deterministic lateral displacement is a technology which utilises the specific arrangement of posts within a channel to precisely control the trajectory of and facilitate separation of particles larger and smaller than a critical diameter (D_c).

Heriot-Watt University, Microfluidic Biotech Group, Institute of Biological Chemistry, Biophysics and Bioengineering (IB3), Riccarton, Edinburgh, UK. E-mail: H.L.Bridle@hw.ac.uk; Tel: +44 (0)131 4513355

Each succeeding row within a constriction is shifted laterally at a set distance from the predecessor, this leads to the creation of separate flow laminae which follow known paths through the device. The separation mechanism of DLD works in that if the centre of a particle is out with the width of the first streamline, it then becomes displaced into the second streamline when negotiating a post. This action continues each time such a particle passes a post, with the particle said to be larger than D_c. Meanwhile, particles that are smaller than D_c remain centred within the first streamline and follow the defined route of this streamline through the device (Fig. 1). Particles smaller and larger than D_c will then be separated from one another along the length of a device.

For 10 years, DLD has been extensively studied, employed and modified by researchers in terms of theory, design, microfabrication and application to develop newer, faster and more efficient separation and processing[20] tools. However, since invention the evolvement and application of this technology has not been reviewed. Due to the wide ranging applications, the diversity in size of particles and cells being separated, the variation in design features, the prospective future applications of this device and the differences in description throughout literature – for example both DLD and deterministic ratchet are used to describe the same technology – a review is long overdue to synthesis the progress to date and to highlight necessary future work.

Firstly, an introduction to the related theory will be provided before design considerations and several of the many applications are discussed – where a comprehensive list of the uses of DLD and the conditions such uses were applied in is detailed in Table 1. This table will allow readers to quickly understand the operating conditions in the referenced applications and we have generated a toolbox to assist with device design for those who are new to the technology.

Some notions to be considered with DLD

The technology of DLD has been developed within the specific conditions encountered at the microscale[1] – the scale of the cell. In this environment certain phenomena which are less prominent at the macroscale, become more influential.[21] For example, phenomena such as diffusion, fluidic resistance and, in particular, laminar flow can influence the performance of microfluidic systems.[21,22] These microscale phenomena are indeed central and influential to the workings of DLD[23] and will therefore be considered in the following sections.

Laminar flow

At the microscale, viscous forces greatly exceed inertial forces in fluid flows[22] and as a result fluid flow is typically laminar and predictable upon introduction to microfluidic systems. If we consider the Navier–Stokes equation for motion of incompressible fluid:[22,23]

$$\rho\left(\frac{\partial v}{\partial t}+v\cdot\nabla v\right)=-\nabla p+\eta\nabla^2 v, \quad (1)$$

Where ρ, v, p and η refer to fluid density, velocity, pressure and viscosity respectively. The non-linear terms $(v\cdot\nabla v)$ on the left side can be disregarded as inertial effects are negligible,[22]

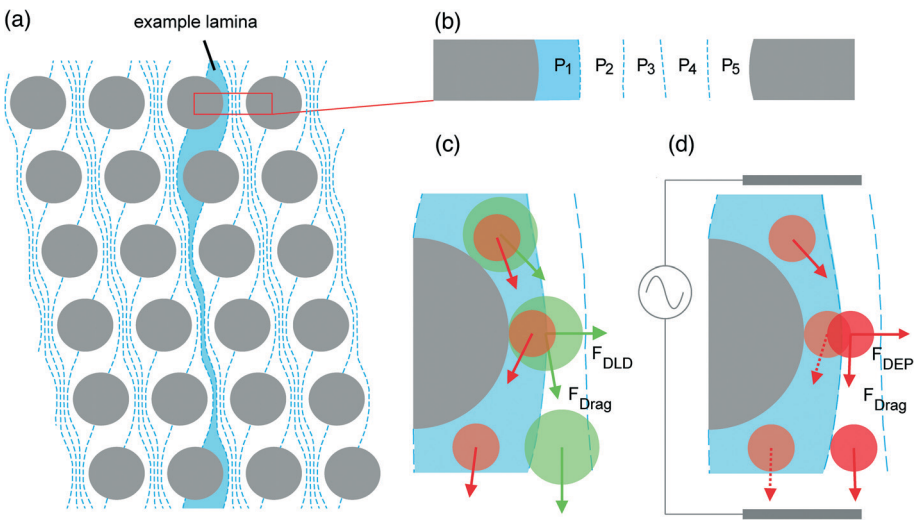

Fig. 1 The streamline orientation and basic principle of DLD with and without an external force. (A) The orientation of flow lamina induced as a consequence of lateral row shifting in a device with N = 5. (B) Position of fluid streamlines (P1, P2, P3…) between two pillars. (C) The normal motion of particles in a DLD; particles smaller than D_c (red) remain within the first streamline influenced by drag force (FDrag) and continue through the device in a zigzagged mode according to the path highlighted by the example lamina. Particles that are larger than D_c (green) are continually displaced into the next streamline at each successive pillar, thus facilitating particle separation. As two particles traverse the length of the device, the distance between them becomes larger. (D) When negative dielectrophoresis is induced in polarisable particles nominally smaller than D_c, they move away from the insulating posts due to dielectrophoretic force (FDEP) and act as if they were larger than D_c, thus entering displacement mode. Adapted from ref. 4 with permission from The Royal Society of Chemistry.

thus giving the Stokes equation:

$$\rho \frac{\partial v}{\partial t} = -\nabla p + \eta \nabla 2v \tag{2}$$

From the Stokes equation, a dimensionless number known as the Reynolds number (Re), which is used to show the ratio of inertial force densities to viscous force densities can be derived[22,23]

$$\mathrm{Re} = \frac{\rho v D_{\mathrm{H}}}{\eta}. \tag{3}$$

In eqn (3), D_{H} represents the hydraulic diameter, which can be calculated using

$$D_{\mathrm{H}} = 2wh/(w + h), \tag{4}$$

where w and h are indicative of the width and height of a microchannel.[24] The Reynolds number is used to characterise the flow behaviour of fluid, where a value above 2000 is considered turbulent and below considered laminar.[22] At the microscale fluid flow is almost always laminar with Re commonly below 1 (ref. 23) and any inertial effects deemed insignificant;[22] this means that when two or more fluid streams meet, they flow in parallel and do not mix except for the effects of diffusion. This feature permits the design of channel geometries to create predictable flow lines, facilitating precise control over the mixing of particles. The placement of pillars within a DLD is an example of how geometry can influence fluid flow to alter the position of suspended particles.

Diffusion

As mentioned previously, parallel, laminar fluid flows within a microchannel mix only by diffusion. For micrometre-sized particles, the effects of diffusion are generally miniscule in a DLD and do not greatly influence overall particle trajectory.[23] However, as particle size decreases diffusivity increases and this may serve to reduce separation efficiency unless flow velocity can be increased.[23]

The Peclet number (Pe) gives the ratio of the rates of convection and diffusion of particles, in terms of the time required to move a certain distance by radial diffusion and axial convection and is defined as[22]

$$\mathrm{Pe} \equiv \frac{vw}{D} = \frac{\text{diffusion time}}{\text{convection time}}. \tag{5}$$

where v and w are representative of flow velocity and microchannel width. The diffusion coefficient is represented by D and the Stokes–Einstein relation can be used to calculate D for spherical particles[23]

$$D = \frac{kT}{6\pi\eta a}. \tag{6}$$

Of the terms in the numerator, k represents the Boltzmann constant and T is the absolute temperature. For the terms in the denominator, a symbolises the hydrodynamic radius of the particle or molecules.

When Pe is high, the rate of convection greatly exceeds the rate of diffusion and this limits the mixing of fluids. The Peclet number is typically high, from 10–10^5, in microchannels[25] and this coupled with low Reynolds numbers results in long mixing times for fluids, giving greater predictability of fluid flow. If we consider the diffusivities of a small protein (40 $\mu m^2\ s^{-1}$) and a mammalian cell (0.02 $\mu m^2\ s^{-1}$), which are typically 5 nm and 10 μm in size[22] and travelling in fluid at 100 $\mu m\ s^{-1}$ in a 100 μm wide channel, then according to eqn (5) the small protein has Pe = 250 whilst it is 500 000 for the mammalian cell. This means that the small protein requires 250 channel widths, or a 2.5 cm long channel and 250 s to diffuse across the width of the channel in fluid travelling at 100 $\mu m\ s^{-1}$. Moreover, this means that in 25 s the protein will have diffused a distance of 10 μm across the channel width. Alternatively, the mammalian cell requires 500 000 channel widths or a 50 m microchannel to diffuse across its width in similar conditions. This illustrates how reducing particle size may lead to more prominent, diffusive effects. This parameter is of first importance in DLD since it could strongly alter the separation efficiency of small particles that tend to diffuse.

Fluidic resistance

Resistance to motion of a fluid within a channel increases as channel dimensions decrease due to an increase in friction between the channel walls and the fluid body. Generally, as channel geometry becomes more complex and surface area to volume ratio increases, so too does resistance (R) and this can serve to restrict flow rate (Q). For pressure-driven flow, the relationship between these properties can be deduced using

$$Q = \frac{\Delta p}{R}. \tag{7}$$

The pressure difference along the channel is symbolised by Δp. It is apparent that a larger value of R in the denominator would serve to decrease Q.

For rectangular microchannels with high aspect ratio, where either channel width or height (h) is greater than the other and when taking channel length (l) into account, the resistance is typically devised using[21]

$$R = \frac{12\eta l}{wh^3}. \tag{8}$$

Alternatively, in a rectangular microchannel with a low aspect ratio ($w \approx h$), resistance is calculated using[21]

$$R = \frac{12\eta l}{wh^3}\left[1 - \frac{h}{w}\left(\frac{192}{\pi^5}\sum_{n=1,3,5}^{\infty}\frac{1}{n^5}\tan h\left(\frac{n\pi w}{2h}\right)\right)\right]^{-1}. \tag{9}$$

When the aspect ratio is particularly large in a DLD, for example in the devices used by Davis[26] where device depth is at least five times larger than the gap between two pillars, the 3D parabolic profile is dominated by the smaller dimension, which is the gap between pillars. In such devices, rearrangement of eqn (8) allows calculation of the resistance in a single gap as

$$R = \frac{12\eta l}{w^3 h}. \quad (10)$$

If we consider a device with a gap between pillars of 10 μm, pillar length of 10 μm and height of 50 μm and then compare this to a device with a gap size of 5 μm – the reduction of the gap size by half, whilst all other parameters remain constant, results in an 8× increase in the resistance according to eqn (10). Although in this specific example it would still be possible to introduce fluid into the system as the pressure requirements are not excessive, the scenario shows how reducing the dimensions of a DLD can cause a marked increase in fluidic resistance, thus affecting possible flow rates and particle sorting times.

DLD principle

DLD or how to use pillars to separate particles

The theoretical basis upon which rigid, spherical particles are separated within a DLD was firstly introduced by Huang *et al.*[1] and developed further by Inglis *et al.*,[3] who both detail that the lateral shifting of each following row of posts at a set distance from the predecessor generates individual streamlines which follow defined paths through the device (Fig. 1A). It is this feature which is utilised to facilitate particle separation. A small section of a DLD with a period $N = 5$ is illustrated in Fig. 1, but streamlines repeat along the full width of an array and continue throughout the length of the device, carrying equal volumetric flow rate.[26] Streamlines directly next to pillars are wider to accommodate more fluid and satisfy the no-slip boundary condition,[27] whilst the central streamline has the smallest width (Fig. 1B) as fluid here travels at the greatest velocity.

According to theory, when two differently sized particles following the same streamline enter the constriction and negotiate a post, assuming that the particles do not alter streamlines and do not interact with one another, a particle smaller than a defined critical diameter (D_c) will remain in the first streamline (Fig. 1C) as its hydrodynamic centre is not out with the width of the first streamline (β). Alternatively, a particle larger than D_c is displaced into the next streamline due to its hydrodynamic centre being out with the boundary of the first streamline – this action continues at every post and is termed displacement mode. Particles larger than D_c are displaced in accordance with the displacement angle (θ) which arises due to lateral row-shifting (Fig. 2). A zigzagged but ultimately straight course through the device ensues for particles smaller than D_c – appropriately termed zigzag mode. Given sufficient time, space and a capable geometry, rigid, spherical particles that are larger or smaller than D_c will be directed to alternate outflows, allowing for collection of separated particles.

The posts contained within one row in a DLD are at a constant centre-to-centre distance from one another, λ, which is the sum of the gap distance, G, and post diameter, D_p. There is a set distance, $\Delta\lambda$, at which each successive row is shifted laterally with reference to its predecessor in a rhombic array (Fig. 2), where rows are perpendicular to the fluid flow with columns tilted. In the titled square array, rows and columns are perpendicular to one another but the array is tilted so that it is not perpendicular to the fluid flow. In the case of the tilted square array, the parameter $\Delta\lambda$ does not exist, however all arguments of DLD theory (to be described) are said to hold true if in this instance $\Delta\lambda$ is calculated as

$$\lambda \tan\theta = \lambda/N. \quad (11)$$

As mentioned, the angle θ develops as a result of lateral row shifting and represents the alignment of each column relative to flow direction. When the posts of row $N + 1$ are in

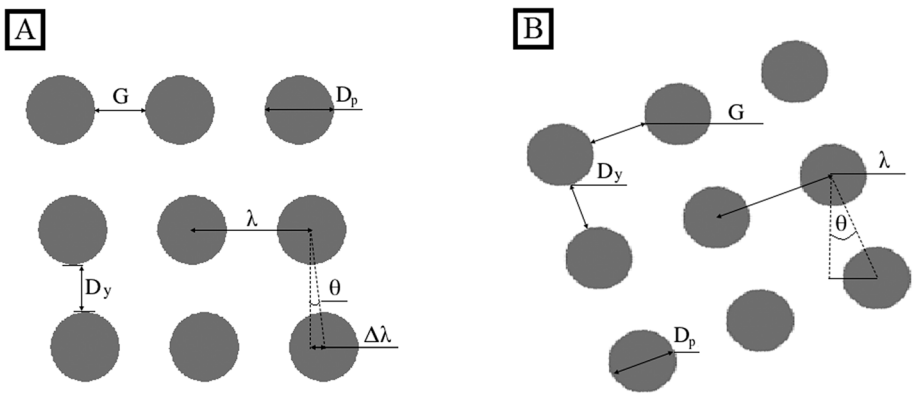

Fig. 2 Important parameters in the design of a DLD. (A) Rhombic array, where rows are perpendicular to fluid flow. (B) Tilted square array, where rows and columns are perpendicular to one another but at an angle to fluid flow. For both configurations, the displacement angle θ develops due to row shifting and particles larger than D_c are displaced according to this angle.

the same lateral position as the first row, the period is said to be N, which is also related to λ and $\Delta\lambda$:

$$N = \frac{\lambda}{\Delta\lambda} \tag{12}$$

For Fig. 1, $N = 5$ and there are N flow lamina or streamlines between two posts, illustrating that the period N dictates the number of streamlines. The inverse of eqn (11) can be used to describe the row shift fraction (ε):

$$\varepsilon = \frac{\Delta\lambda}{\lambda} = \frac{1}{N} = \tan\theta. \tag{13}$$

Analytically, the D_c at which a particle will enter displacement mode is approximated using[3]

$$D_C = 2\beta = 2\alpha \cdot G\varepsilon \tag{14}$$

A unit-less correction factor, α, is used to accommodate non-uniform flow in the DLD and assuming a parabolic flow profile $\alpha = \sqrt{N/3}$ as demonstrated by Beech.[23]

Davis[26] devised an empirical formula for approximation of D_c using over 20 devices with varying gap size and spherical particle size based on a parabolic flow profile. The derived formula is

$$D_C = 1.4G\varepsilon^{0.48}. \tag{15}$$

For some rhombic array devices, the gap between the pillars of a column (D_y) is smaller than G rather than equal and a parallelogram-shaped array becomes apparent. In this instance D_c can be calculated using:[28]

$$D_C = 2\alpha \cdot G\varepsilon' \tag{16}$$

where ε' is:[28]

$$\varepsilon' = \frac{D_y \tan\theta}{\lambda}. \tag{17}$$

Mixed motion

The motion of particles in neither displacement nor zigzag mode has been observed in DLD devices,[1,29] where the net migration angle is not 0° or θ but a value in between. On the basis of 2D flow simulations and experimental data, Kulrattanarak *et al.*[30,31] propose that the phenomenon of mixed motion occurs in a certain subclass of DLD devices due to asymmetric flow lane distribution. This work insinuates that in DLD devices employing a rhombic array (Fig. 2) with $G/D_y \leq 3$ and $0.5D_p/G > 0.2$ the normal symmetry is broken, resulting in an asymmetric flow lane distribution where the first flow lane is smaller than the last ($S_1 < S_N$). Consequently, mixed motion is observable where the particle switches between zigzag and displacement modes.[30,31]

Sidewall effects

Flow profile can become perturbed in the regions between the final column of posts and sidewall, such that D_c changes.[32] In order to minimise such effects the wall can be designed such that it is effectively the final column of posts but where each post in the wall is set at a certain distance from the adjacent column.[32] The wall incorporates posts as not to perturb flow lanes, therefore the sidewall is irregularly shaped rather than a straight wall. In a device separating from left to right the gap between the left sidewall and posts (G_L) is given by

$$G_L = G\sqrt{\frac{n}{N}}. \tag{18}$$

Here, n represents the row number. Meanwhile the gap between the right side wall and posts (G_R) can be derived by

$$G_R = G\sqrt{2 - \frac{n}{N}}. \tag{19}$$

Other factors influencing the critical diameter

There are many observed effects that are known to influence D_c including post size to gap ratio, periodicity and device depth but their exact effects still require quantification. If post diameter decreases but depth, period and gap size remain constant, flow profile gradually becomes more plug-like[23] and D_c becomes reduced. Alternatively, as post size to gap ratio increases flow profile approaches parabola. Critical size is reduced further if post diameter decreases whilst the period increases.[23] Decreased device depth similarly results in smaller D_c, however devices often become too shallow to allow passage of particles before this effect becomes influential.[23]

Numerical simulations of D'Avino suggest that the use of non-Newtonian fluids can allow tuning of D_c; shear-thinning fluids give rise to lower D_c in DLD constrictions when compared to a Newtonian equivalent.[12] The velocity profile is altered due to viscosity thinning, changing flow lane distribution and subsequently reducing D_c. D'Avino derived the following equation to allow calculation of D_c when non-Newtonian fluids are used[12]

$$\frac{D_C}{G} = \frac{A(f)}{A(f) + N - 2}. \tag{20}$$

where f refers to the degree of fluid shear-thinning and $A(f)$ is calculated using

$$A(f) = 1.86 + 1.08f + 1.38f^2. \quad (21)$$

Inertial flow

The effect of inertial flow on separation efficiency has been investigated by Lubbersen *et al.*,[33] where up-scaled systems (70× larger than conventional devices with G = 10 μm) that allow greater throughput were used with increased Re (Re > 1) in comparison to conventional DLD. In this example it appears that the separation of particles on the order of a few hundred microns improves as flow rate and Re increase. This work compared separation efficiency using circular posts, quadrilateral posts and also quadrilateral posts that were mirrored around the central axis (Fig. 3), with the latter giving rise to highest efficiency at increased flow rates. The authors hypothesise that increasing shear-induced lift forces and presence of symmetric vortices behind obstacles in correspondence with larger flow rates has greater influence on particle displacement and consequently, separation efficiency. Where fluids with greater viscosity were used, at the corresponding Re and reduced flow rate, similar results can be observed. In follow up work using up-scaled systems, Lubbersen *et al.* showed using simulations and experimental data that vortices form behind circular posts at Re = 9 and behind quadrilateral posts at Re = 2.[11] This correlates with the previous findings that at the same Re quadrilateral posts give greater separation efficiency, which is dependent upon the presence of vortices and lift forces, in comparison to circular posts. The space occupied by vortices increases as Re increases and serves to introduce more flow lanes between pillars. It is proposed that this effect in conjunction with presence of lift forces causes a reduction in D_c, the deflection of particles into displacement mode and the prevention of zigzag mode. At the highest flow rates investigated, the reduction in D_c due to greater Re was calculated at 14% for circular posts and 24% for quadrilateral posts – where Re was increased from 2 to 30 and 2 to 26 for circular (design 3, Fig. 3) and quadrilateral posts (design 1, Fig. 3), respectively.[11]

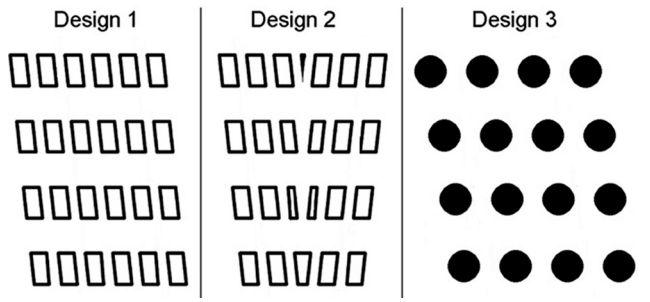

Fig. 3 Geometry of obstacles within a DLD used to investigate the separation efficiency at moderate Reynolds number. Quadrilateral posts, mirrored quadrilateral posts and round posts are used in designs 1, 2 and 3. Adapted from ref. 33 with permission from Elsevier.

Deformable and irregularly shaped particles

For a parabolic flow profile, particles contained within the central section of fluid encounter the greatest shear stress. This also applies in more complex channel geometries, like that of a DLD device,[6] meaning that particles travelling in fluid at the centre between two pillars experience the greatest shear stress. The theory of DLD has been developed using rigid, spherical particles for which size is not altered by the shear forces typically encountered within such devices. However, the hydrodynamic radius of a soft particle like a cell may decrease as it passes between two objects and deforms.[34] This is a feature that has been observed by researchers where soft cells such as red blood cells (RBCs) have been processed in DLD systems.[7,23] Therefore the important separation parameters, namely row shift fraction (ε) and gap (G), should be designed to separate based on effective size rather than actual size as separation efficiency will be reduced if effective size is lower than the designed critical size of the device. Predicting the critical size of a deformable particle is challenging as it is influenced by factors including the mechanical properties of the particle, orientation of the particle, particle–post or particle–particle interaction and how specific experimental conditions (*e.g.* flow rate) contribute to the shear stress acting upon a particle.[23] Consequently, design iterations might be required to optimise performance.

Determining the shear stress acting upon a particle brings complexity, as a particle alone causes flow perturbation – for example, particles that are much smaller than the gap do not tend to cause significant perturbation but particles slightly smaller than the gap are known to cause large perturbations and if soft may be capable of deformation, which would further influence perturbation.[23] Additionally, particle–post interactions may cause particle deformation and flow perturbation.

When irregularly shaped particles flow between pillars in a DLD they tend to become orientated in a manner that makes their smallest dimension the critical dimension.[23] Additionally, the mode of transport also influences particle behaviour and consequently the effective size; particles tend to rotate continuously due to asymmetric viscous drag when in displacement mode, meanwhile particles in zigzag mode instead deform, as the effective shear experienced varies between flow lanes.[34] The shear rate, deformation and relaxation time of a particle influences which of deformation or rotation influence dominates.[34] In order to limit the range of possible orientations of irregularly shaped particles within a DLD, Holm *et al.* reduced device depth.[17] This work demonstrates the use of a very shallow constriction to ensure that RBCs pass posts with their width as the critical dimension, rather than thickness. This effect ensures that the critical dimensions of RBCs and trypanosomes are not similar and facilitates their separation.

Particle concentration

At high particle concentrations DLDs are more likely to clog as an increase in the number of particle–post and particle–particle

interactions occurring is inevitable. As particle concentration increases, the flow profile becomes more perturbed and this can change D_c within a device to affect separation efficiency.[23] If we consider a wide distribution of small and large particles at high concentration, many small particles will not be able to negotiate posts according to theory due to the dense concentration of particles overall, which will result in their displacement out of the first streamline and thus influencing their trajectory. One can expect that such effects would be more prominent in a device processing rigid, spherical particles than a device handling soft, deformable particles of similar hydrodynamic radius and concentration,[23] due to the inability of rigid, spherical particles to alter formation in such when faced with objects in this environment. Beech[23] describes the processing of blood at concentrations just below 100%, however it is apparent in Table 1 that particles and cells are commonly diluted in solutions including surfactants before DLD processing to limit the effects described above.

Design considerations

Post shape

Many researchers have investigated the effect of changing post shape within a DLD, in order to improve performance whilst retaining several of the advantageous properties of this technology. Posts have been implemented or modelled in DLD's in a variety of shapes (see Fig. 4 and Table 1.0) including triangular,[35] streamlined,[5] I-shaped,[36] airfoil-shaped,[37] diamond[37] and quadrilateral posts,[11] which were discussed in the previous section relating to inertial flow conditions. One of the main reasons for changing shape is that circular posts are known to have zones at the very top of the post where the flow velocity is zero and this means that particles often become trapped. Loutherback *et al.* used triangular posts to reduce the effects of clogging and alter the regular, symmetric flow profile such that the device has a different D_c when flow is in reverse than when flow is forward.[35] An additional property of this change is that the use of triangular posts reduces the resistance within the device, so that less pressure is required to generate the same flow rate.

The use of streamlined posts was modelled and proposed by Beech as a method of reducing the areas surrounding circular pillars with zero flow velocity, to increase recovery and reduce clogging.[5]

The use of I-shaped posts is aimed at separating non-spherical and/or deformable particles within a DLD. Zeming *et al.* developed this particular post shape in order to induce a series of rotations in non-spherical particles which serve to increase hydrodynamic radius whilst passing I-shaped obstacles within the constriction, thus facilitating separation.[36]

Diamond and airfoil posts were modelled by Al-Fandi *et al.* with a view to reducing the clogging and deformation issues that soft, deformable particles experience when negotiating circular posts, where the author concluded that airfoil posts were most suitable.[37] Airfoil post simulations indicated that flow exerts less variation in velocity gradient, very low forces at the post surface and higher values of tangential forces when compared to circular and diamond posts; leading the author to conclude that this design would inhibit the clogging, sticking or deformation of particles in this constriction. However, there appears to be no experimental data related to the efficiency of airfoil posts, perhaps due to the complexity concerned with manufacturing such a device.

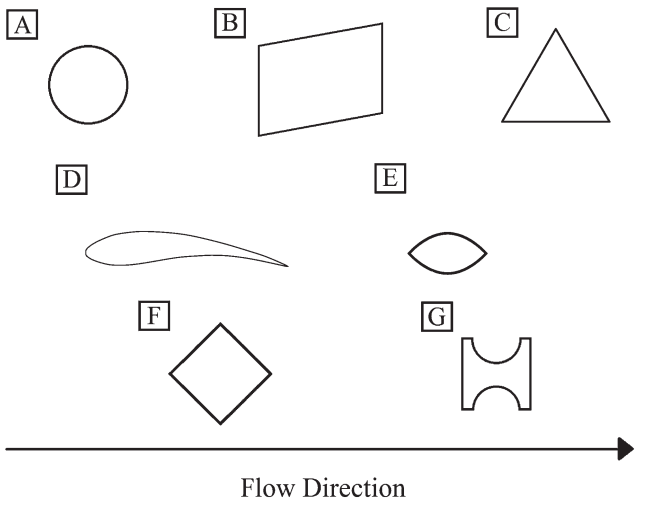

Fig. 4 Variation in post shapes used experimentally or simulated within a DLD and an indication of post orientation in reference to fluid flow direction. (A) Circular (B) quadrilateral (C) triangular (D) airfoil (E) streamlined (F) diamond (G) I-shaped.

Multiple separations

Multiple arrays are employed when it is desirable to have more than one size-based separation within a DLD constriction. By having several arrays with sequentially decreasing D_c it is possible to separate particles within various size thresholds. For devices with a small separation range, it is important to ensure that particles no larger than G of the final array enter the device, as this increases the risk of clogging. Holm *et al.* designed an inline filter within the sample inlet to ensure particles no larger than G of the final array enter the device,[17] thus limiting the effects of clogging.

Particle outflow and collection

If it is desirable to separate particles of a wide range of sizes or to increase the throughput of a device, then separate non-clogging outflows can be implemented to ensure larger particles cannot clog further down the device[19] (see Fig. 5). Inglis *et al.* detail that outflow channels should be designed to ensure that their pressure drop is the same as the next array, as to avoid alterations in flow behaviour which may affect separation efficiency.[19] As particles are separated in space within the DLD constriction it is possible to collect particles at as many different outflows as is required (or is practically possible) at the end of the device, however it is important to ensure that the resistance within each

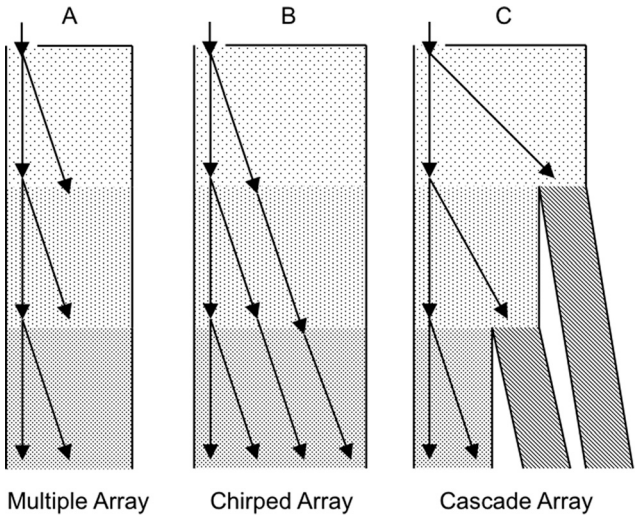

Fig. 5 DLD device designs with several separation arrays. (A) A multiple array for use where the largest particle diameter is no larger than the gap size of the final array. (B) A chirped array where row shift fraction (ε) is varied to increase separation range and reduce clogging in comparison to the multiple array. As ε increases the displacement angle (θ) also increases; see eqn (13). (C) A cascade array with separate non-clogging outflows to increase the separation range further. Black arrows indicate particle trajectories. Reproduced from ref 26 with permission.

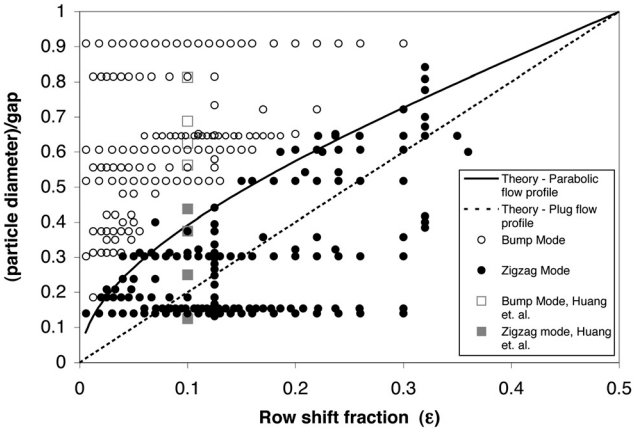

Fig. 6 Experimental points of the particle diameter divided by the gap, G, *versus* the row shift fraction, ε. For the work of Inglis *et al.*[3] (in black) and that of Huang *et al.*[1] (in grey), open points represent bump mode and solid points represent zigzag mode. Zigzag mode particles follow the streamlines, while bump mode particles follow the array slope, ε. Adapted from ref. 3 with permission from The Royal Society of Chemistry.

subdivision of the outlets is similar as to maintain and not perturb flow profile, thus facilitating separation.[23,26]

Toolbox: instructions for designing a DLD

1. Critical diameter. – Define the critical diameter (D_c) desired. Particles larger than D_c will be deviated.

2. Post shape. – Circular, triangular, I-shaped, square shapes are proposed in the literature among others (see Table 1 and/or Fig. 4).

– Calibration curves are proposed in ref. 3 for circular posts and in ref. 35 for triangular posts.

– Triangular posts allow a larger gap G between the posts than circular ones.

– I-shaped or square posts induce rotation of non-spherical particles to increase their effective diameter.

3. Array geometry (circular posts). – Circular posts, the "common shape"

– Based on D_c, define the gap G and row shift fraction ε.[3] See Fig. 6 for the ratio of particle diameter divided by G *versus* ε to approximate the particle trajectory.

Note:. – $D_{c\ min} = G/5$.[7]

– Maximum dynamic range in a chirped array 3–5.[7]

– Typical displacement angles (θ) are 1 to 6°.[19]

– Refer to ref. 35 for design help for triangular posts which allow a larger gap G for similar D_c and ε.

4. Post size. – Large posts with small gaps give a more parabolic profile while small posts with large gaps give a more plug-flow profile.[35]

– Tall posts lead to a higher throughput, but the post aspect ratio is limited by the moulding step. Polydimethylsiloxane (PDMS) posts with an aspect ratio that is more than 2 have an unacceptably high probability of tipping over during assembly. An aspect ratio of 2 for an injection moulded plastic device is at the limit of current manufacturing methods. Extremely large posts, relative to the gap also reduce the critical size, whereas extremely small posts are expected to increase the shear rate.[38]

5. Edge correction.[32]– Left boundary correction

$$G_L = G\sqrt{\frac{n}{N}}$$

Where G_L is the width of the gap between the left sidewall and the first pillar of the nth row, within an array with period N.

– Right boundary correction

$$G_R = G\sqrt{2-\frac{n}{N}}$$

Where G_R is the width of the gap between the last pillar in the nth row and right sidewall.

6. Inlet and outlet design.[23,26]– Sample and buffer inlet divisions should have similar resistance to ensure parallel flow enters the device.

– Non-clogging outflows of cascade arrays should be designed to ensure that their pressure drop is the same as the next array.

– Divisions of outlet channels should have identical resistance to maintain the profile of flow leaving the constriction.

– Lateral separation is determined by the displacement angle and device length – this calculation will determine outlet positioning.

7. Note on materials. – Problem of cell adhesion to the posts in PDMS reported in the literature,[39] see surface treatment in Table 1.

– Significant deformation of gap size has been reported for standard glass–PDMS devices.[40]

– Flow velocity profile between heterogeneous surfaces in *e.g.* glass–PDMS devices has been reported as asymmetrical for certain aqueous fluids.[40]

– PDMS devices deform considerably under pressure.[38]

Application

A summarisation of the main applications, including biomedical uses, proposed in the literature using the DLD technique is given in Table 1. Where this information was available, Table 1 describes the range of particle sizes being separated, post shape, design parameters, manufacturing details, surface pre-treatment, flow rates used, buffer employed, external forces applied and provides information on the separation efficiency of the referenced work.

Pre-treatment, buffers and non-clogging agents

The presence of numerous posts in a microchannel greatly increases the surface area-to-volume ratio meaning that particles are more likely to bind to a surface. In a DLD, such binding to pillars or walls would not only result in particle losses, but could perturb flow lanes and ultimately clog a device. Therefore, several researchers pre-treat devices with surfactants or other similar chemicals and/or make sample containing fluids and/or buffer solutions which limit particle–surface binding but also particle–particle binding. To provide an example, Inglis *et al.*[38] introduced a solution of DI water and 0.1% (v/v) Tween-20 through the device before performing any particle studies. The presence of polyethylene glycol (PEG)[8] and sodium dodecyl sulphate (SDS)[4] in containing fluids and buffers, where beads are the target particles, shows how researchers are attempting to ensure particles remain unbound. Furthermore, the inclusion of bovine serum albumin (BSA)[7,18,39] and phosphate buffered saline (PBS)[7,18,39,41,42] in containing fluids and buffers where live cells or blood is used serves to restrict any binding. In whole blood separation studies, Li *et al.*[42] added heparin as an anti-coagulant to assist in the division of blood into its constituent parts (Fig. 7). The formation of bubbles can also affect device performance by perturbing flow lanes and the placing of devices in vacuum (for 2 hours in this instance) before use can restrict bubble formation.[19]

Throughput

If we analyse the sample flow rates used where particles of several microns are separated in the described applications (Table 1); for devices with circular posts we see that the flow rate typically ranges from 0–1 μL min^{-1}, whilst those documenting increased flow rates are either separating larger cells or particles and/or employing the use of triangular posts, or use acoustic forces, where virtual posts are generated thus permitting a sample flow rate of 4.1 μL min^{-1} (ref. 8) (described in following section). Flow rates of up to 2 mL min^{-1} (ref. 41) and 10 mL min^{-1} (ref. 18) are documented in devices separating circulating tumour cells (CTCs) and employing triangular posts, whilst the release of oil droplets containing *Saccharomyces cerevisiae* is documented at 600 μL h^{-1}.[40] In contrast, shallow devices are incapable of permitting the same volumetric flow rate as deeper devices. For instance the work of Holm *et al.*[17] required the separation of the irregularly shaped trypanosomes from blood and extremely shallow device was fabricated in order to facilitate this however, flow rates of only 1 nL s^{-1} were possible.

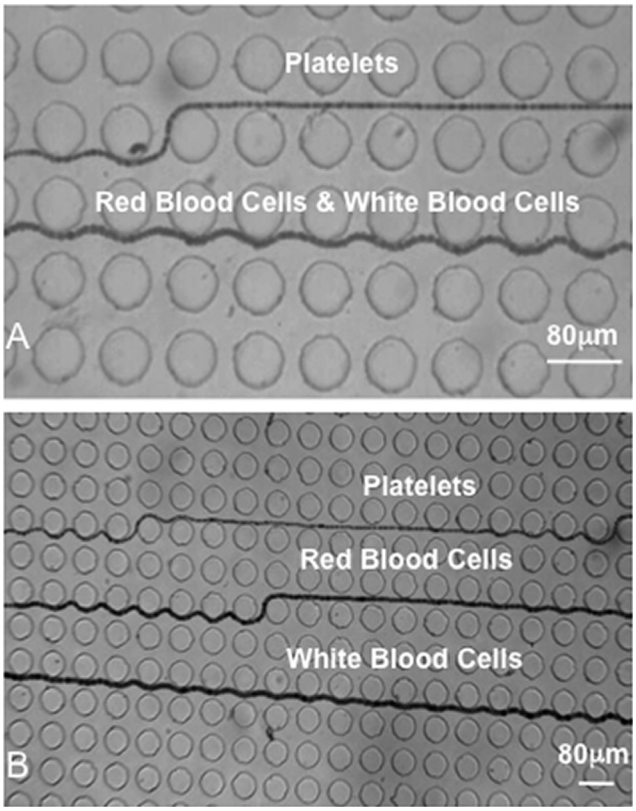

Fig. 7 Trajectory of platelets, red blood cells and white blood cells through two stages of a whole blood separation DLD device with heparin used as an anti-coagulant. Sample and buffer flow rates were 0.1 μL min^{-1} and 1 μL min^{-1} respectively. (A) Separation of platelets from red blood cells and white blood cells through stage one of the device. (B) Separation of platelets, red blood cells and white blood cells in stage two of the device. Reproduced with permission from ref. 42 © 2007 IEEE.

Comments on separation efficiency

In the process of generating this review we have come to realise that much of the literature presenting DLD demonstrates well the principle, however often fails to clearly detail the recovery rates and purity of samples processed in the described devices. Of the applications in Table 1 that do provide such information, many report over 90% separation

Table 1 Application and conditions of analyses utilising DLD technology

	Application	Critical size	Post shape	Design parameters	Manufacturing details	Pre-treatment	Containing fluid/buffer	Flow speed/driving pressure/flow rate	External forces (comments)	Recovery rate/ purity/resolution/ related comments
BEADS	300 and 500 nm, 5.0 and 6.6 μm, 6.6 and 7 μm (ref. 8)	Tuneable	None	h = 15 and 45 μm, θ ~ 45°	Polydimethyl-siloxane (PDMS) chamber bonded to 0.5 mm thick lithium niobate substrate with 5/250 nm chrome aluminium IDTs arrayed on top	—	Deionized water (DI) with 0.2% polyethylene glycol/none	4.1 μL min^{-1} for 5, 6.6 and 7 μm beads 0.45 to 1.8 μL min^{-1} for 300 and 500 nm beads	Acoustic/electric forces to create virtual pillars	99.1 ± 0.7% and 99.3 ± 1.3% of 5.0 μm and 6.6 μm successfully separated with DEP. 99.5 ± 0.5% and 97.3 ± 2.7% using SAW. 80–90% separation of 6.6 μm and 7 μm particles. 87% separation of 500 nm particles from 300 nm
	0.40 to 1.03 μm (ref. 1)	0.64 μm to 1.10 μm	Circular	D_{post} = 6.4 μm, G = 1.6 μm, ε = 0.1	Silicon device manufactured using deep reactive ion etching (DRIE)	—	Aqueous solution/none	~40 μm s^{-1} and ~400 μm s^{-1} (30 to 300 mbar)	None	Resolution of ~20 nm
	1.1 to 3.1 μm (ref. 45)	~1.4 to 1.9 μm	Right isosceles triangular posts	D_{post} = 6 μm, G = 4 μm, θ = 5.71°, h = 10 μm	Silicon by DRIE sealed with a PDMS-coated glass slide	—	—/—	~250 μm s^{-1}	None	—
	1.9 to 3.8 μm (ref. 35)	D_c/G from 0.25 to 0.55 in Fig. 2.b, D_c ~ 1.6 to 3.5 μm	Triangular	θ = 2.86° to 11.46° (Fig. 2.b), ε = 0.05 to 0.2 (tan θ), D_{post} = 4.7 μm, G = 6.3 μm, w = 3.4 mm, l = 16.8 mm	Silicon by DRIE sealed with a PDMS-coated glass slide	—	—/—	~100 μm s^{-1}	None	—
	2 to 10 μm (ref. 4)	6 to 2 μm	Circular	l = 25 mm, ε = 0.1, G = 12 μm, D_{post} = 30 μm, h = 34 μm	PDMS and glass using replica molding/	—	—/0.5× TBE, 0.1% (w/v) SDS with 2.5% PVP	Between 90 and 260 μm s^{-1} for 5 μm beads (10 to 100 mbar)	Coupled with DEP	Author comments that D-DLD gives poorer resolution than DLD
	2.1, 4.2 and 5.7 μm (ref. 43)	Array 1: D_c = 3.1 μm. Array 2: D_c = 4.6 μm measured by electron microscope (were designed to be 3.5 and 5 μm)	Circular	Inlet 1 – 820 μm wide, inlet 2 – 5180 μm wide. 2 arrays: array 1 – 33.7 mm long, G = 10.5 μm, θ = 2.86°. Array 2 – 16.9 mm long, G = 10.5 μm, θ = 5.7°. 3 outlets	PDMS-glass device manufactured using soft lithographic techniques	Flushed with 0.2 μm filtered DI water for 20 min at 5 psi	2.1, 4.2 and 5.7 μm beads diluted at ratio 2 : 1 : 2 in DI water containing 1 g L^{-1} F108 giving total concentration of 12 × 10^6 beads ml^{-1}/buffer = 0.2 μm filtered DI water	Beads introduced at 5 psi	None	99% recovery of 4.2 μm particles and 96% removal of 2.1 μm and 5.7 μm particles

Table 1 *(continued)*

Application	Critical size	Post shape	Design parameters	Manufacturing details	Pre-treatment	Containing fluid/buffer	Flow speed/driving pressure/flow rate	External forces (comments)	Recovery rate/ purity/resolution/ related comments
2.3 to 22 μm (ref. 3)	—	Circular	Up to 22 combinations, ε = 0.01 to 0.33, G = 12 to 38 μm, D_{post}/G = 0.32 to 1.36, h = 25 μm, l (bump array) = 2 cm	Features in silicon, device in PDMS coated glass cover slips	Devices soaked in a 2 g L^{-1} solution of Pluronic F108	—/—	~500 to 1500 μm s^{-1} (0.03 to 0.14 bar)	None	—
Stainless steel balls (3, 6, 6.4, 7.1 mm in diameter) in glycerol[2]	—	Circular	D_{post} = 7.8 mm, G = 16 mm, θ = 13–30°	Lego®	—	—/Glycerol	—	None	—
3.4, 4.0, 5.0, or 6.0 μm (ref. 31)	—	Circular	Devices placed in module with entry and exit channels to connect syringes, 2 inlets and outlets of equal width, h = 40 μm, w = 15 mm, l = 15 mm, D_{post} = 3.2–8 μm, G = 8–9 μm	Silicon devices manufactured using lithography and DRIE	0.25 wt% Synperonic PEF108 solution pumped through for 30 min	Bead stock suspensions diluted with MilliQ water to volume concentration of 0.05%/MilliQ water	Buffer and sample fluids introduced at 4 μL h^{-1}.	(Analysis of mixed motion)	—
Silica particles 4.32, 10, 15, 20 μm (ref. 10)	—	Circular	h ~ 40 μm, D_{post} = 17.5 μm, G = 22.5 μm	SU-8 device spin coated onto microscope slide using standard photolithography procedures	—	Particles suspended in 1 mM KOH solution/—	—	Gravity-driven DLD	At a driving angle of 14° resolution is ~1.35 (see paper for resolution equation)
5.7 to 11.9 μm (ref. 9)	Tuneable	None	w = 1.7 mm, l = 2.3 mm, h = 14.4 μm, θ ~ 21°	Electrodes deposited on glass wafer by sputtering. Reactive ion etching used to fabricate spots on electrode arrays. PDMS device produced from SU-8 master using replica moulding and bonded to glass *via* plasma treatment	—	PBS diluted in DI+ 0.2 w/w Tween 20/—	Buffer 0.2–0.3 μL min^{-1} sample 0.1 μL min^{-1}	DEP to create virtual pillars	Depending on electric field applied work demonstrates over 99% separation purity for all PS particles used
10 to 16 μm (ref. 44)	14 to 18 μm	Circular	ε = 0.05, G = 54 μm	PDMS device manufactured	—	0.001% mass/ volume suspen-	~500 μm s^{-1}	Coupled with mechanical	100% separation

Table 1 *(continued)*

	Application	Critical size	Post shape	Design parameters	Manufacturing details	Pre-treatment	Containing fluid/buffer	Flow speed/driving pressure/flow rate	External forces (comments)	Recovery rate/ purity/resolution/ related comments
					using standard rapid prototyping and replica molding techniques		sion of polystyrene beads/0.1% solution of Pluronics F127		stretching	
	209 to 277 μm and 309 to 532 μm (ref. 33)	For designs 1, 2 – D_c = 400 μm, for design 3 – D_c = 330 μm	Circular/ quadrilateral/ mirrored quadrilateral	G = 0.56 or 0.6 mm, D_y = 1.13 or 1.80 mm, quadrilateral obstacles – 0.8 × 1.6 mm, D_{post} of round obstacles 0.68 mm, ε = 0.25 or 0.17, h = 2.5 mm	Polyether ether ketone (PEEK) device manufactured by milling and placed in stainless steel module with Polymethyl methacrylate (PMMA) lid	Chamber washed initially with demi water + 20% v/v glycerol + 1.5% w/v SDS at 80 mL min^{-1}	Experiments 1 & 3: demineralised (demi) water + 20% v/v glycerol + 1.5% w/v SDS. Experiment 2: demi water + PEG-400 to give solution with 164 or 220 mPa s^{-1} viscosity. Note – only one inlet so bead/buffer introduced together as mixture	20–275 mL min^{-1}.	(Inertial effects in system at elevated Re)	Separation efficiency ratio of 47 (see paper for derivation of ratio)
BLOOD	WBCs (5–20 μm) from RBCs (~8 μm × 2 μm) and plasma[7]	From 3 μm to 9 μm	Circular	13 functional regions, D_{post} = 12 μm, G = 10 μm, ε = 0.04 to 0.4, h ~ 25 μm	Standard photolithography to construct silicon devices. Bosch silicon etching process used to give near vertical sidewalls. Devices coated in fluorosilane vapour and sealed with glass coverslips coated in PDMS	2 g per liter solution of the triblock copolymer F108	Blood/PBS with 1% BSA and 0.09% sodium azide	~1000 μm s^{-1} (cell) (blood flow 0.3 nL s^{-1}, pressure ~0.1 bar)	None	99% of RBCs in channel 1. 99% of granulocytes and 99.6% of all WBCs displaced into channels 2 and 3
	WBCs from RBCs[9]	Tuneable	None	w = 1.7 mm, l = 2.3 mm, h = 14.4 μm, θ ~ 21°	Electrodes deposited on glass wafer by sputtering. Reactive ion etching used to fabricate spots on electrode arrays. PDMS device produced from SU-8 master using replica	—	Blood diluted 10 times in 0.3 M sucrose buffer with 0.2% EDTA/—	Buffer 0.1 μL min^{-1} sample 0.01 μL min^{-1}	DEP to create virtual pillars	Over 99% separation purity of WBCs from RBCs

Table 1 *(continued)*

Application	Critical size	Post shape	Design parameters	Manufacturing details	Pre-treatment	Containing fluid/buffer	Flow speed/driving pressure/flow rate	External forces (comments)	Recovery rate/ purity/resolution/ related comments
				moulding and bonded to glass *via* plasma treatment					
WBCs from RBCs[6]	~8 μm	Circular	h = 20 μm, l = 7 mm, w = 1.8 mm, G = 14 μm, D_{post} = 46 μm	PDMS device made using DRIE moulds mounted on glass slides	—	Blood diluted (2, 5 and 10 times) with Ficoll-Paque Plus/—	0.08 μL min^{-1} sample 0.4 μL min^{-1} buffers	None (impact of the blood dilution and freshness)	Initial WBC : RBC = 1 : 43 final ratio = 1 : 38 giving ~88.4% separation efficiency
WBCs, RBSs and platelets from blood[42]	3.8 and 6.1 μm	Circular	w = 1.6 mm, l = 6.8 mm 2 stages stage 1: G = 20 μm, D_{post} = 60 μm, ε = 0.025 stage 2: G = 20 μm, D_{post} = 60 μm, ε = 0.0625	PDMS devices made using soft lithography from DRIE silicon moulds	PBS+ heparin at 1 μL min^{-1} for 10 min	Blood diluted 50 times in PBS + heparin/—	0.1 μL min^{-1} sample 1 μL min^{-1} buffers	None	The ratio of separated RBCs to platelets to WBCs was found about 470 : 36 : 1, compared to the ratio of 500 : 50 : 1 in normal whole blood
RBCs from blood[36]	3.33 μm for circular, between 2.5 and 3 μm for I-shaped	Circular/ square/ I-shaped	3 inlets, 3 outlets with 40 outlet subchannels, D_{post} = 15 μm, G = 10 μm, l ~ 20 mm, w ~ 2 mm, h ~ 15 μm, θ = 2.86°	Silicon-PDMS/ photolithography	1% w/v Pluronic F127 in deionized water for 30 min	Blood diluted 10 times in PBS/PBS	Blood 0.2 μL min^{-1}, buffers 0.5 μL min^{-1}	None (impact of the pillar shape)	100% separation of RBCs from blood
RBCs depending on their size, morphology, deformability[46]	From 3 to 9 μm	Circular	13 sections, D_{post} = 20 μm, G = 12 μm, ε = 0.025 to 0.27, h = 10.84 μm and h = 4.27 μm	PDMS device bound to fluorisilane-coated silicon wafer created using standard lithography, DRIE and sandblasting (entry/exit holes)	0.2% PLL(20)-g[3.5]-PEG(2) in DI water and left to rest for at least 20 min, then rinsed with autoMACS®	Blood diluted 5 times in autoMACS® with sodium salicylate and TritonX-100/ autoMACS® with EDTA and BSA	From 30 μm s^{-1} to 18 cm s^{-1} (driving pressure form 5 to 800 mbar)	None (Impact of the depth)	—
Enrichment of leukocytes from blood[38]	D_{c1} = 7.3 μm D_{c2} = 4.5 μm	Circular	2 arrays and 6 parallel devices (3 mirroring pairs) – no buffers. Array 1: D_{post} = 22 μm, G = 22 μm, ε = 0.05, h = 40 μm, w = 836 μm, l = 26 367 μm array 2: D_{post} =	Multilayer SU-8 and PDMS device manufactured using standard lithography and plasma bonding	De-ionized water + 0.1% (v/v) Tween-20 for 5 min for beads. AutoMACS® buffer for 5 min for blood	Whole or diluted blood in AutoMACS®/ none	Whole undiluted blood ~115 μL min^{-1} atm^{-1} (0.2 atm)	None	Capture of 98% and approximately ten-fold enrichment of leukocytes in whole blood

Table 1 *(continued)*

Application	Critical size	Post shape	Design parameters	Manufacturing details	Pre-treatment	Containing fluid/buffer	Flow speed/driving pressure/flow rate	External forces (comments)	Recovery rate/ purity/resolution/ related comments
			22 μm, G = 13 μm, ε = 0.05, h = 40 μm, w = 840 μm, l = 25 868 μm						
$CD4^+$ T helper lymphocytes from other WBC[42]	23 μm	Circular	G = 47 μm, ε = 0.15, D_{post} = 13 μm	PDMS devices made using soft lithography from DRIE silicon moulds	PBS+ heparin at 1 μL min^{-1} for 10 min	WBCs in PBS (1×10^6 cells mL^{-1}) with antibodies coated beads (25 μm)/—	0.2 μL min^{-1} sample 1.2 μL min^{-1} buffers	(Attached antibodies to WBC for a subtype separation)	100% separation of 25 μm beads with 91% recovery of T lymphocytes
Platelets (~3.2–3.6 μm in diameter, ~0.9–1.1 μm thick), from blood[19]	D_c = 2.3–5.3 μm in array 2	Circular	Array 1: G = 17 μm array 2: 11 steps, D_{post} = 20 μm, G = 6–17 μm, ε = 0.01–0.125, h = 18 μm	PDMS-glass device	Deionized water +2 g L^{-1} Pluronic F108 and placed under vacuum for 2 h	Blood in anti-coagulant citrate dextrose with PE-conjugated antihuman CD41/Auto MACS® buffer	Blood 0.8 nL min^{-1}, 14 kPa	None	—
Undiluted blood plasma from whole blood[7]	From 4 to 1 μm	Circular	3 functional regions 1: l = 17.6 mm, w = 1.1 mm, D_{post} = 10 μm, θ = 2.8°, G = 20 μm 2 : l = 21 mm, w = 910 μm, D_{post} = 9 μm, θ = 1.7°, G = 9 μm 3: l = 28.7 mm, w = 680 μm, D_{post} = 6 μm, θ = 0.85°, G = 5 μm/ device with serpentine regions to remove sorted particles	Standard photo-lithography to construct silicon devices combined with Bosch silicon etching. Devices coated in fluorosilane vapour and sealed with PDMS-coated glass coverslips	2 g per liter solution of the triblock copolymer F108	Blood/PBS with 1% BSA and 0.09% sodium azide	(Blood flow 0.4 μL min^{-1}, pressure 0.3 bar)	None	100% removal of all components greater than 1 μm from blood plasma
Circulating tumor cells (15–30 μm) from blood (other cells 2–15 μm)[18]	7 μm	Triangular	1 input, 2 outputs, mirrored array. w = 2.5 mm, l = 25 mm, D_{post} = 58 μm, G = 42 μm, θ = 2.86°, h = 60 μm	Silicon wafer sealed with a PDMS-coated glass cover slide – standard lithography	1× PBS, 1% BSA, and 1 mM EDTA	Cell suspension in buffer or diluted blood (between 5 and 20 times) with buffer/none (3.75×10^6 cells mL^{-1})	1.5 to 150 cm s^{-1} (0.1 to 10 mL min^{-1}) 4 atm at 10 mL min^{-1}	None	Captured over 85% of CTCs from blood
Circulating tumour cells	~5–6 μm	Circular/ triangular	One inlet, three outlets, mirrored	Standard photolithography	—	Cultured cells in PBS	0.01 to 2 mL min^{-1}	None (tests with 5 human cancer	90% capture yield and more than

Table 1 *(continued)*

	Application	Critical size	Post shape	Design parameters	Manufacturing details	Pre-treatment	Containing fluid/buffer	Flow speed/driving pressure/flow rate	External forces (comments)	Recovery rate/ purity/resolution/ related comments
	(15–25 μm, 1 in 10^9 cells) from diluted peripheral blood (other cells 5–15 μm)[41]			design. l = 35 mm, w = 3.5 mm, h = 30 μm, circular posts: D_{post} = 50 μm, G = 25 μm, θ = 3.2° triangular posts: D_{post} = 25 μm, G = 25 μm, θ = 3.8°	and soft lithography – PDMS bonded to glass sides		(10^5 cells mL^{-1}) or cultured cells in 10 times diluted blood with physiological saline (~10^4 cells mL^{-1})/none		cell lines- comparison between triangular and circular posts)	50% capture purity
PATHOGENIC CELLS	*E. coli* (0.5 μm in diameter, 2 μm long) in DI[36]	1.12 μm for the circular shape	Circular/ I- shaped	D_{post} = 6 μm, G = 4 μm, l ~ 20 mm, w ~ 500 μm, h ~ 8 μm, θ = 2.00°	Silicon device manufactured by standard lithography and DRIE, PDMS cover layer bound to device by plasma treatment	1% w/v Pluronic F127 for 30 min	Cell culture in DI/DI (8 × 10^7 cells mL^{-1})	0.3 μL min^{-1} for the wider flow stream, 0.08 μL min^{-1} for the narrow stream, 0.05 μL min^{-1} for the sample stream	None	Overall efficiency not given but author states that bacteria tend to stick to posts in ESI
	Trypanosomes (~2.5 μm × 30 μm) from human blood[17]	From 3 to 9 μm	Circular	13 sections, ε = 0.025 to 0.27, D_{post} = 20 μm, G = 12 μm, h = 4, 11 and 33 μm	PDMS device generated using replica molding from SU-8 master, patterned PDMS bound to PDMS cover using plasma treatment	0.2% PLL(20)-g[3.5]-PEG(2) in DI water for at least 20 min before rinsing with DI water for another 20 min	Parasites and blood diluted 20 times in autoMACS® (without blood serum for experiments with blood and parasites)/ autoMACS®	~600 μm s^{-1} (~1 nL s^{-1})	None (Impact of the depth)	99.5% sorting efficiency (fraction of trypanosomes captured with lateral displacement such that 99% of the RBCs are rejected by the device)
	Trypanosomes (3.7–5.8 μm in effective diameter)[37]	2.7 μm	Circular	D_{post} = 20 μm, G = 10 μm, θ = 2.86°	Not detailed	—	—	—	None	—
	Mature and immature spores of *Aspergillus brasiliensis* (0–10 μm).[43]	Array 1: D_c = 3.1 μm. Array 2: D_c = 4.6 μm measured by electron microscope (were designed to be 3.5 and 5 μm)	Circular	Inlet 1 – 820 μm wide, inlet 2 – 5180 μm wide. 2 arrays: array 1 – 33.7 mm long, G = 10.5 μm, θ = 2.86°. Array 2 – 16.9 mm long, G = 10.5 μm, θ = 5.7°. 3 outlets	PDMS-glass device manufactured using soft lithographic techniques	Flushed with 0.2 μm PBS for 15 min at 10 psi	4.4 × 10^6 spores ml^{-1} PBS with 0.1% Tween-20/ 0.2 μm filtered DI water	10 psi/total volumetric flow through of 40 μL min^{-1}	None	Two- to three-fold increase in purity of spores
DROPLETS	Water drops (3.6 to 11.7 mm) in oil[47]	—	Circular	D_{post} = 7.8 mm, G = 16 mm θ = 0–45°	Lego®	—	Water/oil	—	Gravity	—
	Droplets (11–30 μm in diameter) with	24 μm	Circular	D_{post} = 60 μm, ε = 0.1, G = 60 μm, h = 30 μm	PDMS device manufactured by standard lithog-	Treated with a coating agent (Aquapel, PPG	(PBS or *S. cerevisiae* in YPD medium	10 μL h^{-1} PBS, 500 μL h^{-1} oil (30 μm	None	Outlet 6 contained 99.9% large droplets, whereas

Table 1 *(continued)*

	Application	Critical size	Post shape	Design parameters	Manufacturing details	Pre-treatment	Containing fluid/buffer	Flow speed/driving pressure/flow rate	External forces (comments)	Recovery rate/ purity/resolution/ related comments
	S. cerevisiae encapsulated in oil[40]				raphy from SU-8 mould, plasma treatment used to bond device to glass slide	industries) and flushed with air	(2×10^6 cells mL^{-1})/oil for droplet generation)/oil	droplets), 30 μL h^{-1} PBS, 600 μL h^{-1} oil (10 μm droplets) and 5 mL h^{-1} buffer		at the central outlet has >97% small droplets
OTHER	Bacterial artificial chromosomes (61 and 158 kb)[1]	1.39 μm based on Davis corr.	Circular	G = 3 μm, D_{post} = 5 μm, ε = 0.1	Fused silica device	—	—/—	~20 μm s^{-1}	Electric fields	Resolution of 12%
	H1975 epithelial cell fractionation (10–40 μm)/ H1975 epithelial cell line and the 3T3 fibroblast cell line (13.7 ± 3.0 μm)[39]	15 μm	Circular	3 inlets, 6 outlets G = 37.5 μm, ε = 0.1, D_{post} = 50 μm	PDMS device manufactured using standard soft lithography techniques	Devices flushed with ethanol, then rinsed with PBS followed by an injection of 1% BSA. The 1% BSA was allowed to adsorb in the device for 30 min before rinsing with PBS.	Cell in PBS (5×10^5 cells mL^{-1})/PBS note: clogging issues for higher cell concentration (1×10^6 cells mL^{-1})/	200 μL min^{-1} sample, 500 μL min^{-1} buffers	None	~90% recovery rate of H1975 epithelial cells and 97% separation efficiency of recovered cells = 87.3% of total cells separated

Notes: the column headings of Table 1 have been ordered in a chronological manner from the desired application to design considerations, manufacture, experimental details, any external forces applied and details of separation efficiency. Depending on application, the referenced work has been categorised as beads, blood, pathogenic cells, droplets or other and where possible the works contained under each category are listed in ascending order of size. For applications enlisted within the blood category, those using alike cells have been grouped together to improve legibility for the reader.

Table 2 Notation and Units

Term	Meaning	Unit/value
ρ	Density	kg m^{-3}
v	Velocity	m s^{-1}
p	Pressure	Pa
η	Viscosity	Pa s
D_H	Hydraulic diameter	—
w	Width	m
h	Height	m
l	Length Note: in Fig. 8 l refers to post centre–centre distance to satisfy notation of ref. 17	m
D	Diffusion coefficient	cm^2 s^{-1}
k	Boltzmann constant	1.38×10^{-23}
T	Absolute temperature	K
α	Hydrodynamic radius	m
Q	Flow rate	m^3 s^{-1}
R	Fluidic resistance	N s m^{-5}
Δp	Pressure difference	Pa
D_c	Critical diameter	m
$D_{c\ min}$	Minimum critical diameter	m
β	Width of first streamline	m
θ	Displacement angle Note: in Fig. 8 θ represents driving angle	Degrees
n	Periodicity of array	—
n	Row number	—
S_n	Streamline number	—
G	Gap size	m
D_p	Post diameter	m
D_y	Distance between posts in one Row and those in another	m
λ	Centre-to-centre post spacing	m
$\Delta\lambda$	Distance that each successive row is shifted laterally	m
ε	Row shift fraction	—
ε'	Row shift fraction in devices with $D_y < G$	—
G_L	Gap between left sidewall and posts	m
G_R	Gap between right sidewall and posts	m
f	Degree of fluid shear thinning	—
F_{Drag}	Drag force	N
F_{DEP}	Dielectrophoretic force	—
b_c	Critical angle	Degrees
Re	Reynolds number	—
Pe	Peclet number	—
psi	Pounds per square inch	lbf in^{-1}
DLD	Deterministic lateral displacement	—
IMS	Immuno-magnetic separation	—
FACS	Fluorescence-activated cell sorting	—
PFF	Pinched flow fractionation	—
HDF	Hydrodynamic filtration	—
WBC	White blood cell	—
RBC	Red blood cell	—
CTC	Circulating tumour cell	—
PDMS	Polydimethylsiloxane	—
DI	Deionized	—
PEG	Polyethylene glycol	—
SDS	Sodium dodecyl sulfate	—
BSA	Bovine serum albumin	—
PBS	Phosphate buffered saline	—
AC	Alternating current	—
IDT	Interdigital transducer	—
DRIE	Deep reactive ion etching	—
DEP	Dielectrophoresis	—
TBE	Tris/borate/EDTA buffer	—
PVP	Polyvinylpyrrolidone	—
KOH	Potassium hydroxide	—
Demi	Demineralized	—
PEEK	Polyether ether ketone	—
PMMA	Polymethyl methacrylate	—
EDTA	Ethylenediaminetetraacetic acid	—
YPD	Yeast extract peptone dextrose	—

efficiency for target particles. For example, the preliminary tests in the work of Inglis *et al.*,[43] which uses DLD to remove waste and enrich target particles, details the 96% removal of waste (2.1 μm and 5.7 μm beads) and 99% enrichment of target particles (4.2 μm beads). Processing of fungal spores in the same device resulted in a two- to three-fold increase in the purity of *Aspergillus brasiliensis*. The work of Green *et al.*[39] reports the 97% separation of recovered H1975 epithelial cells from 3T3 fibroblasts within the designed DLD however, with only ~90% of H1975 recovered the actual efficiency is nearer 87.3%. The reader is referred to Table 1 for any known details of separation efficiency in other referenced applications and Table 2 for details of the notation and units listed in this paper.

A note on microfabrication

Most devices are fabricated using standard lithography procedures, as is apparent within the manufacturing details column of Table 1, and they are predominantly PDMS devices manufactured from a silicon resist.[6,40,42] However there are some devices within the referenced applications that have silicon[7,10] or fused silica[1] as the main constituent, or that are PDMS devices but manufactured by replica moulding.[4,17,44] The values of design parameters selected by investigators to suit and enable their desired separation are also indicated within the manufacturing details column of Table 1.

DLD coupled with external forces

Several researchers have investigated the application of external forces with DLD to improve the efficiency and/or functionality of devices and/or allow utilisation of particle properties other than size for separation. For example, the application of mechanical strain to a DLD manufactured of PDMS has been demonstrated, where the applied strain increased the distance between pillars allowing tuning of D_c and increasing the range of the device.[44] By bonding either half of the PDMS device to a glass slide, the device could be clamped in a chuck and subsequently stretched – the 100% separation of 10 μm and 16 μm particles was demonstrated in a stretched device.

Beech *et al.* used pillars manufactured of an insulator material placed between electrodes to modulate an electric field throughout the whole constriction.[4] By tuning the applied, low frequency AC electric field which ran perpendicular to the fluid flow direction, it was possible to continuously deflect polystyrene beads smaller than D_c into displacement mode when experiencing negative dielectrophoresis (Fig. 1D).

In this instance beads are effectively repelled from the pillars, causing their displacement out of the existing streamline.

Chang and Cho developed a device with electrode pillar arrays to create a tuneable, negative dielectrophoretic effect within a DLD device, where a voltage was applied to the electrode pillars *via* an electrode backbone.[9] Tuning of the voltage enabled the separation of 6, 8, 10 and 12 μm particles, with the larger particles being forced into displacement mode and smaller particles flowing through the device in zigzag mode. Furthermore, the 99% separation of WBCs from RBCs was exhibited using this device.

Devendra and Drazer used gravity to induce particle movement through a DLD constriction by simply tilting the microfluidic device at a set force angle for size-fractionation of mixed particle populations.[10] Smaller particles have a smaller critical angle (b_c) than large particles, and therefore migration can be controlled by controlling the offset angle as is outlined in Fig. 8. Particles move with an average migration angle of $\alpha = 0°$ with $b_c = l \sin(\theta_c)$, where l is the post centre-to-centre distance and θ_c the transition angle. When $b_c < l \sin(\theta_c)$, particles no longer migrate with $\alpha = 0°$, thus facilitating size-based separation. The device is tuneable in that changing the offset angle renders particles within a different range susceptible to the separation but the highest resolution of ~1.35 was given at a driving angle of 14°.

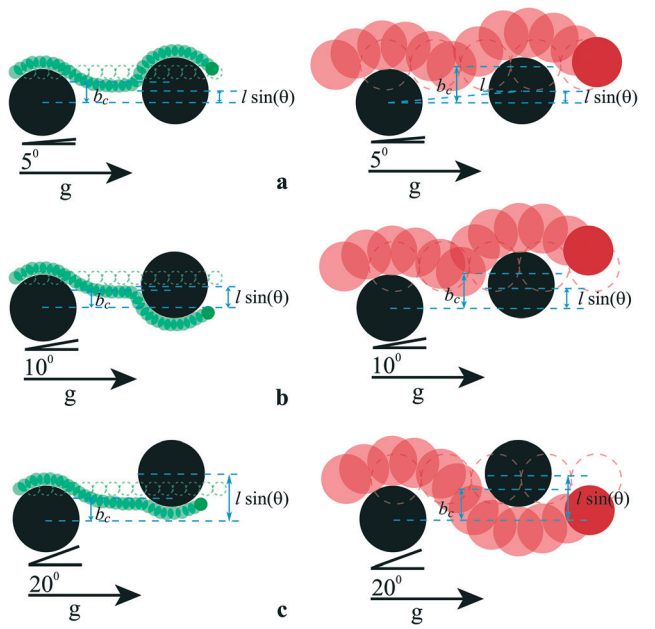

Fig. 8 Schematic trajectories of 4.32 μm (green, left) and 15 μm (red, right) particles colliding with two consecutive cylindrical posts (black) of 20 μm, separated centre-to-centre by distance l. The driving angles are $\theta = 5°$ (a), $\theta = 10°$ (b) and $\theta = 20°$ (c). The dotted circles show the trajectories of the particles in the absence of obstacles. The two particles have two different values of the impact parameter, b_c. Initially, both particles move with $\alpha = 0°$. Each particle then transitions out of this locking direction when $b_c < l \sin(\theta c)$. Transitions occur at different θ. The middle cartoon is representative of a separative case. Adapted with permission of Devendra and Drazer.[10] Copyright 2012 American Chemical Society.

Collins *et al.* used a virtual DLD system with interdigital transducers (IDT's), which produce surface acoustic waves at an angle to flow direction, rather than pillars to enable continuous size-based separation of particles in the micrometer and sub-micrometer range.[8] Principally, this system works by trapping particles larger than D_c in the force field produced by the IDT's, which is at 45° to the flow direction. Smaller particles are not sufficiently affected by the force field and consequently separation ensues. The device is tuneable in that the applied voltage can be selectively controlled – the >97% separation of 5 μm from 6.6 μm particles and then ~87% separation of 500 nm from 300 nm particles in the same device demonstrates this.

Conclusion

This paper reviewed 10 years of evolution in terms of microfluidic designs and applications related to Deterministic Lateral Displacement. This passive separation technique relies on the fluid motion encountered in presence of posts arrayed with a specific geometry in the channel. By controlling the post geometry, shape and channel design, the separation can be deterministic in the sense that particles with an effective diameter larger than a critical value are deviated, contrary to smaller particles that follow an ultimately straight path within the device.

To date, this technique has been used for the separation of a wide range of particles, from white blood cells to droplets, and from nanometre-sized to millimetre-sized particles. By relying only on hydrodynamics, flow rates as high as 10 mL min^{-1} have been reported in the literature for the separation of cancer cells from blood corresponding to *one of the highest flow rates reported for this purpose using microfluidics*. However, fluid volumes processed by DLD's are typically very small (0–1 μL min^{-1}), therefore we expect that in the future work detailing the stacking or running of devices in parallel will be published, in order to increase the capability of this separation technique and its suitability to biomedical applications, for example. On the subject of suitability of devices to specific applications, researchers should detail the recovery rates and purity of target particles from the tested devices, as this information is missing from most publications.

Specific care is required when dealing with DLD since clogging by means of particle–particle or particle–surface interactions can occur but also high resistances can limit its practical implementation. Some of the above limitations can be overcome by adding external forces to the process such as dielectrophoresis or acoustic forces for creating a virtual DLD and avoiding the presence of physical posts in the device.

Clearly though, design considerations are thus crucial for this technique and the most significant devices designed were presented in this review. However, and without compromising its interesting potential for particle separation, there is not yet a "one fits all" solution and one should refer to the most related literature to adapt DLD to the targeted application. By gathering studies related to DLD in a

single review, this process will hopefully be simplified, potentially enhancing new applications since there is still much to explore. Additionally, in this paper, a toolbox was proposed to summarize the main design parameters requiring of consideration and to serve as a design aid to those unfamiliar with the technique.

Strong efforts have been reported during the last decade to adapt this technique to the separation of non-spherical biological matters resulting in the consideration of new posts shapes or new designs for the channel, depending on the particles to be separated. In terms of future work, it is expected that work will commence to further characterise device performance where inertial or non-Newtonian effects are present and where target particles are irregularly-shaped and/or deformable as this will enable more appropriate design of a wider range of applications.

The large majority of publications to date refer to the use of DLD alone on chip; however it is conceivable that more devices will be designed and integrated with upstream and/or downstream processes. For example, Liu *et al.*[41] demonstrate particle separation using DLD, before target cells are captured downstream. Perhaps the next stage for developers of DLD is to show that this technology is truly capable of integrated lab-on-chip applications.

Acknowledgements

HB would like to acknowledge The Royal Academy of Engineering/EPSRC for her research fellowship. JM would like to acknowledge the Science and Technology Facilities Council for provision of PhD funding. Both HB and MJ would like to acknowledge EU funding for the project "AQUAVALENS: protecting the health of Europeans by improving methods for the detection of pathogens in drinking water and water used in food preparation".

References

1 L. R. Huang, E. C. Cox, R. H. Austin and J. C. Sturm, *Science*, 2004, **304**, 987–990.
2 M. Balvin, E. Sohn, T. Iracki, G. Drazer and J. Frechette, *Phys. Rev. Lett.*, 2009, **103**, 078301.
3 D. W. Inglis, J. A. Davis, R. H. Austin and J. C. Sturm, *Lab Chip*, 2006, **6**, 655–658.
4 J. P. Beech, P. Jonsson and J. O. Tegenfeldt, *Lab Chip*, 2009, **9**, 2698–2706.
5 J. P. Beech, *Deterministic Lateral Displacement Devices*, MSc, Lund University, 2005.
6 S. Zheng, R. Yung, Y.-C. Tai and H. Kasdan, *Deterministic lateral displacement MEMS device for continuous blood cell separation*, 2005.
7 J. A. Davis, D. W. Inglis, K. J. Morton, D. A. Lawrence, L. R. Huang, S. Y. Chou, J. C. Sturm and R. H. Austin, *Proc. Natl. Acad. Sci. U. S. A.*, 2006, **103**, 14779–14784.
8 D. J. Collins, T. Alan and A. Neild, *Lab Chip*, 2014, **14**, 1595–1603.
9 S. Chang and Y.-H. Cho, *A continuous multi-size particle separator using negative dielectrophoretic virtual pillars induced by a planar spot electrode array*, 2007.
10 R. Devendra and G. Drazer, *Anal. Chem.*, 2012, **84**, 10621–10627.
11 Y. Lubbersen, J. Dijkshoorn, M. Schutyser and R. Boom, *Sep. Purif. Technol.*, 2013, **109**, 33–39.
12 G. D'Avino, *Rheol. Acta*, 2013, 1–16.
13 A. A. S. Bhagat, H. Bow, H. W. Hou, S. J. Tan, J. Han and C. T. Lim, *Med. Biol. Eng. Comput.*, 2010, **48**, 999–1014.
14 E. L. Jackson and H. Lu, *Curr. Opin. Chem. Eng.*, 2013, **2**, 398–404.
15 J. Autebert, B. Coudert, F.-C. Bidard, J.-Y. Pierga, S. Descroix, L. Malaquin and J.-L. Viovy, *Methods*, 2012, **57**(3), 297–307.
16 M. Kersaudy-Kerhoas, R. Dhariwal and M. Desmulliez, *IET Nanobiotechnol.*, 2008, **2**, 1–13.
17 S. H. Holm, J. P. Beech, M. P. Barrett and J. O. Tegenfeldt, *Lab Chip*, 2011, **11**, 1326–1332.
18 K. Loutherback, J. D'Silva, L. Liu, A. Wu, R. H. Austin and J. C. Sturm, *AIP Adv.*, 2012, **2**, 042107.
19 D. W. Inglis, K. J. Morton, J. A. Davis, T. J. Zieziulewicz, D. A. Lawrence, R. H. Austin and J. C. Sturm, *Lab Chip*, 2008, **8**, 925–931.
20 K. Loutherback, *Microfluidic Devices for High Throughput Cell Sorting and Chemical Treatment*, Doctor of Philosophy, Princeton University, 2011.
21 D. J. Beebe, G. A. Mensing and G. M. Walker, *Annu. Rev. Biomed. Eng.*, 2002, **4**, 261–286.
22 T. M. Squires and S. R. Quake, *Rev. Mod. Phys.*, 2005, **77**, 977–1026.
23 J. P. Beech, *Microfluidics Separation and Analysis of Biological Particles*, PhD, Lund University, 2011.
24 J. J. Hawkes, R. W. Barber, D. R. Emerson and W. T. Coakley, *Lab Chip*, 2004, **4**, 446–452.
25 H. A. Stone, A. D. Stroock and A. Ajdari, *Annu. Rev. Fluid Mech.*, 2004, **36**, 381–411.
26 J. A. Davis, *Microfluidic Separation of Blood Components Through Deterministic Lateral Displacement*, Doctor of Philosophy, Princeton University, 2008.
27 E. Lauga, M. P. Brenner and H. A. Stone, in *Experimental Fluid Mechanics.*, Springer, 2007, ch. 19.
28 D. W. Inglis, *Microfluidic Devices for Cell Separation*, Doctor of Philosophy, Princeton University, 2007.
29 B. R. Long, M. Heller, J. P. Beech, H. Linke, H. Bruus and J. O. Tegenfeldt, *Phys. Rev. E: Stat., Nonlinear, Soft Matter Phys.*, 2008, **78**, 046304.
30 T. Kulrattanarak, R. Van der Sman, Y. Lubbersen, C. Schroën, H. Pham, P. Sarro and R. Boom, *J. Colloid Interface Sci.*, 2011, **354**, 7–14.
31 T. Kulrattanarak, R. van der Sman, C. Schroën and R. Boom, *Microfluid. Nanofluid.*, 2011, **10**, 843–853.
32 D. W. Inglis, *Appl. Phys. Lett.*, 2009, **94**, 013510.
33 Y. Lubbersen, M. Schutyser and R. Boom, *Chem. Eng. Sci.*, 2012, **73**, 314–320.
34 K. Adolfsson, *Master's Thesis*, Department of Solid State Physics, Lund Institute of Technology, 2011.
35 K. Loutherback, K. S. Chou, J. Newman, J. Puchalla, R. H. Austin and J. C. Sturm, *Microfluid. Nanofluid.*, 2010, **9**, 1143–1149.

36 K. K. Zeming, S. Ranjan and Y. Zhang, *Nat. Commun.*, 2013, **4**, 1625.
37 M. Al-Fandi, M. Al-Rousan, M. A. Jaradat and L. Al-Ebbini, *Robot. Comput. Integr. Manuf.*, 2011, **27**, 237–244.
38 D. W. Inglis, M. Lord and R. E. Nordon, *J. Micromech. Microeng.*, 2011, **21**, 054024.
39 J. V. Green, M. Radisic and S. K. Murthy, *Anal. Chem.*, 2009, **81**, 9178–9182.
40 H. N. Joensson, M. Uhlén and H. A. Svahn, *Lab Chip*, 2011, **11**, 1305–1310.
41 Z. Liu, F. Huang, J. Du, W. Shu, H. Feng, X. Xu and Y. Chen, *Biomicrofluidics*, 2013, **7**, 011801.
42 N. Li, D. T. Kamei and C.-M. Ho, *On-chip continuous blood cell subtype separation by deterministic lateral displacement*, 2007.
43 D. W. Inglis, N. Herman and G. Vesey, *Biomicrofluidics*, 2010, **4**, 024109.
44 J. P. Beech and J. O. Tegenfeldt, *Lab Chip*, 2008, **8**, 657–659.
45 K. Loutherback, J. Puchalla, R. H. Austin and J. C. Sturm, *Phys. Rev. Lett.*, 2009, **102**, 045301.
46 J. P. Beech, S. H. Holm, K. Adolfsson and J. O. Tegenfeldt, *Lab Chip*, 2012, **12**, 1048–1051.
47 T. Bowman, J. Frechette and G. Drazer, *Lab Chip*, 2012, **12**, 2903–2908.

